Revista Mexicana de Astronomía y Astrofísica, **51**, 255–265 (2015)

ON THE EQUILIBRIUM OF A DISTORTED HETEROGENEOUS ELLIPSOIDAL MASS. II: THE STABILITY OF HOMOGENEOUS SPHEROIDAL FIGURES

J. U. Cisneros Parra,[1] F. J. Martínez Herrera,[2] and J. D. Montalvo Castro[2]

Received 2015 July 22; accepted 2015 August 13

RESUMEN

Empleando las ecuaciones del virial de segundo orden y el super-potencial, estudiamos la estabilidad a segundo armónico de las figuras líquidas homogéneas esferoidales reportadas en I, dotadas de un movimiento interno de velocidad angular diferencial. Esta cantidad, que para el equilibrio era suficiente con especificarla sólo sobre la superficie frontera del cuerpo, ahora es requerida en todo su interior, con dos alternativas físicamente aceptables: constante sobre la superficie de cilindros; o constante sobre discos; estas dos distribuciones se someten al criterio de Goldreich para estabilidad local. Tal como en la secuencia de Maclaurin, se encuentra que en cada una de nuestras series hay una figura de frecuencia neutra y una región de inestabilidad.

ABSTRACT

Employing second order virial equations and super-potential, we investigate stability to the second-harmonic of the spheroidal homogeneous liquid figures reported in I, whose equilibrium is due to an internal motion of differential rotation. The angular velocity, which for equilibrium it was enough to be specified on the body's boundary surface, is now required throughout its interior, two alternatives being physically acceptable: constant over cylinder surfaces; or constant over disks; these two distributions are subjected to Goldreich's criterium for local stability. Just as in Maclaurin's sequence, a figure of neutral frequency and a region of instability are found in each of our series.

Key Words: gravitation — hydrodynamics — stars: rotation

1. INTRODUCTION

Having constructed the self-gravitating *spheroidal* homogeneous liquid figures reported in Cisneros et al. (2015), hereinafter Paper I, whose equilibrium is due to an internal motion of differential angular velocity, we now investigate their stability to second-harmonic for which virial techniques and super-potential are employed. In Paper I it was enough to specify the angular velocity distribution on the body's boundary surface for establishing equilibrium, now it is required throughout its interior. The surface equation of the distorted spheroid is

$$x^2 + y^2 + \frac{z^2}{e_3^2} + d\,\frac{z^4}{e_3^4} = 1, \qquad e_3 = \frac{a_3}{a_1}, \tag{1}$$

where d is a parameter independent of x, y and z, with $d > -1/4$ in order for the surface to be closed; a_1, a_2 (in the current case $a_1{=}a_2$) are semi-axes, but a_3 is the third semi-axis only in the limit $d \to 0$; the true third semi-axis is z_M, which is proportional to e_3 $(= a_3/a_1)$; a_1 is taken as a scale factor. The general solution for equilibrium consists of series of series.

[1]Facultad de Ciencias, Universidad Autónoma de San Luis Potosí, México.
[2]Instituto de Física, Universidad Autónoma de San Luis Potosí, México.

The reason for using such a surface responds to our wish to construct figures of exact equilibrium for a heterogeneous model composed of two concentric ellipsoids, which was fruitless using the purely quadratic surface equation; for spheroids, on the other hand, the model works well. Just as in Maclaurin's sequence a figure of neutral frequency and a region of instability occur; these two results are found in each of our series with the difference that instead of eccentricity we work with semi-axes. We use

$$x \to a_1\, x, \quad y \to a_1\, y, \quad z \to a_1\, z, \tag{2}$$

for the coordinates of points on the surface; and

$$x_1 \to a_1\, x_1, \quad x_2 \to a_1\, x_2, \quad x_3 \to a_1\, x_3, \tag{3}$$

for the coordinates of the reference point.

2. THE EQUILIBRIUM EQUATION

The equation governing our body's equilibrium is Bernoulli's theorem for steady state (Dryden; 1956 and Paper I),

$$V + \frac{p}{\rho} + \frac{1}{2}\omega^2\, r = \text{cte.}, \qquad r = x_1^2 + x_2^2, \tag{4}$$

which holds for any streamline, where V is the gravitational potential, p is the pressure, ω is the angular velocity, and ρ is the density. Applying the boundary condition of zero pressure at the body's boundary surface, the above equation reduces to $V + \Omega\, r = V_p$, where V_p refers to the pole potential, and Ω ($\sim \omega^2$) is the (squared) angular velocity distribution; these quantities are normalized (see § 5).

3. THE POTENTIAL AND SUPER-POTENTIAL

In Paper I an expression for V was empirically established whose precision, although reasonably good, was valid only at the body's boundary surface. In the current context, we shall proceed differently. As before we assume that V, and now the super-potential χ, are given by

$$V = \alpha_s(x_3^2) + \alpha_x(x_3^2)\, r + \alpha_y(x_3^2)\, r^2, \qquad \chi = \beta_s(x_3^2) + \beta_x(x_3^2) r + \beta_y(x_3^2) r^2, \tag{5}$$

where

$$r = x_1^2 + x_2^2,$$

and we demand that they satisfy Poisson's equation (Chandrasekhar & Lebovitz, 1962):

$$\triangle V = -4\pi, \qquad \triangle \chi = -2\, V. \tag{6}$$

Inserting equations (5) in (6) we determine the variables α and β:

$$\begin{aligned}
\alpha_s &= \frac{16}{15}\alpha_0 \left(\sqrt{x_3^2}\right)^5 + \frac{8}{3}\alpha_1 x_3^4 - \frac{4}{3}\alpha_2 \left(\sqrt{x_3^2}\right)^3 - 2\alpha_3 x_3^2 + 2\alpha_4 \sqrt{x_3^2} - 2\pi x_3^2 + \alpha_5, \\
\alpha_x &= -\frac{16}{3}\alpha_0 \left(\sqrt{x_3^2}\right)^3 - 8\alpha_1 x_3^2 + 2\alpha_2 \sqrt{x_3^2} + \alpha_3, \\
\alpha_y &= 2\alpha_0 \sqrt{x_3^2} + \alpha_1, ,
\end{aligned} \tag{7}$$

and

$$\begin{aligned}
\beta_s &= \beta_5 + \frac{4}{15}\left(\sqrt{x_3^2}\right)^5 (\alpha_2 + 4\beta_0) + \frac{1}{3} x_3^4 (2\alpha_3 + 8\beta_1 + \pi) - \frac{1}{105} 16\alpha_0 \left(\sqrt{x_3^2}\right)^7 \\
&\quad - \frac{2}{3}\alpha_4 \left(\sqrt{x_3^2}\right)^3 - \frac{1}{15}(8\alpha_1)\, x_3^6 + (-\alpha_5)\, x_3^2 - \frac{4}{3}\beta_2 \left(\sqrt{x_3^2}\right)^3 - 2\beta_3 x_3^2 + 2\beta_4 \sqrt{x_3^2}, \\
\beta_x &= \beta_3 + \frac{16}{15}\alpha_0 \left(\sqrt{x_3^2}\right)^5 - \frac{2}{3}\alpha_2 \left(\sqrt{x_3^2}\right)^3 + \frac{8}{3}\alpha_1 x_3^4 - \alpha_3\, x_3^2 - \frac{16}{3}\beta_0 \left(\sqrt{x_3^2}\right)^3 \\
&\qquad\qquad - 8\beta_1 x_3^2 + 2\beta_2 \sqrt{x_3^2}, \\
\beta_y &= \beta_1 - \frac{2}{3}\,\alpha_0 \left(\sqrt{x_3^2}\right)^3 - \alpha_1\, x_3^2 + 2\beta_0 \sqrt{x_3^2},
\end{aligned} \tag{8}$$

where $\alpha_0, \ldots, \alpha_5$ and $\beta_0, \ldots, \beta_5$ are arbitrary constants.

For a particular equilibrium configuration, i.e., for fixed d and z_M (z_M measures the figure's flattening), the constants α and β can be determined through a fit procedure involving, say, 64 random points located all in the first quadrant—taking advantage of the symmetry— and we can then compute V and χ at each of these points, where χ is given by the integral relation[3]

$$\chi = -\int |\mathbf{x} - \mathbf{x}'|\, d\tau', \qquad d\tau' = dx'_1 dx'_2 dx'_3.$$

Next we fit equations (5) to these 64 values, thus obtaining the parameters α and β.

4. THE ANGULAR VELOCITY DISTRIBUTION

In studying our body's equilibrium the angular velocity distribution in equation $V + \Omega\, r = V_p$ (see Paper I), was taken as:

$$\Omega = \frac{\alpha_s(x_3^2)}{r} + \alpha_x(x_3^2) + \alpha_y(x_3^2) r, \tag{9}$$

where the variables $\alpha_s, \alpha_x, \alpha_y$ are related to equation (7); more precisely, these quantities were established taking $V_p - V$ in equation (5), instead of V, and letting $\alpha_s(z_M) = 0$; hence, Ω depends on five parameters: $\alpha_0, \ldots, \alpha_4$.

To carry out our stability analysis, Ω must be specified throughout the body's interior, and an adequate method for extending this—and the other quantities related to the equilibrium—from the boundary surface inward must be conceived resulting in two physically acceptable alternatives: (a) we can choose it constant over the surface of cylinders; or (b) constant over disks. Once the desired extension of V and Ω is accomplished, the corresponding extension of p follows.

(a) The cylindrical angular velocity distribution.

To examine this case we note that on the surface Ω depends on r ($= x_1^2 + x_2^2$) and x_3. Eliminating x_3 by means of the surface equation written as $r = 1 - x_3^2/e_3^2 - d x_3^4/e_3^4$, we obtain

$$\Omega(r, x_3^2) = \Omega_r(r) = \frac{\alpha_s(x_3^2)}{r} + \alpha_x(x_3^2) + \alpha_y(x_3^2) r \Big|_{x_3^2 = \frac{e_3^2}{2d}\left(\sqrt{-4d\, r + 4d + 1} - 1\right)}; \tag{10}$$

we will take this $\Omega_r(r)$ as the angular velocity prevailing for all r within the body, so that it is constant over cylinders of radius r coaxial with the rotation axis. This kind of distribution will fit for all of our spheroidal figures.

b) The disklike angular velocity distribution.

If instead of x_3 we choose to eliminate r in equation (9), we obtain

$$\Omega(r, x_3^2) = \Omega_x(x_3^2) = \frac{\alpha_s(x_3^2)}{r} + \alpha_x(x_3^2) + \alpha_y(x_3^2) r \Big|_{r = 1 - \frac{x_3^2}{e_3^2} - d\frac{x_3^4}{e_3^4}}, \tag{11}$$

which is valid for all points with coordinate x_3. Hence, the loci of the points with $x_3 = $ const. are disks whose axis is the rotation axis, and Ω is now constant over disks ('rigid' disks) of height x_3. This kind of distribution would only fit for a limited number of our figures.

4.1. *Cylindrical distribution vs. disklike distribution*

According to Bernoulli's equation (4) any of the two distributions—both compatible with the continuity equation—influences the pressure field. Numerical results show that disklike distributions lead to stronger pressure; this is because cylindrical distributions are more effective to support the gravitational force (except when the angular velocity decreases from the equator to the rotation axis). The two distributions are in priciple suitable for all of our figures; nevertheless, as we show in what follows, only for negative d the disklike distribution is acceptable beyond a certain e_3 (see § 6, Figure 1), so that both distributions can coexist beyond that value of e_3. To decide which distribution is pertinent, we will subject our models (even though they are liquid) to Goldreich's local stability criterion for gaseous stars.

[3]The potentials are normalized so that $G\rho = 1$, see § 5.

4.2. *Goldreich's criterion for local stability*

Goldreich's criterion for local stability of gaseous stars is (Goldreich & Schubert, 1967)

$$\frac{\partial}{\partial s}\left(s^2\omega\right) - \frac{k_s}{k_z}\frac{\partial}{\partial z}\left(s^2\omega\right) > 0, \tag{12}$$

where $s^2 = x^2 + y^2$, ω ($\sim \sqrt{\Omega}$) is the angular velocity, k_s and k_z being wave numbers relative to radial and z dimensions, respectively, and where it is generally assumed that $\partial\omega/\partial z > 0$—so that as usual ω increases from the equator to the pole—; this might imply that for sufficiently large k_s/k_z the value of the second term in the above inequality can override the first, making its left-hand side negative. Hence, for local stability the angular velocity distribution should be such that $\partial\omega/\partial z = 0$, and Goldreich's criterion reduces to

$$\frac{\partial}{\partial s}\left(s^2\omega\right) > 0, \tag{13}$$

and the cylindrical distribution $\Omega_r(r)$ can in principle satisfy it. The disklike distribution $\Omega_x(x_3^2)$ conforms to equation (13), but not necessarily to equation (12). If $\partial\Omega_x/\partial x_3 > 0$, which most of our models fulfill (see § 6), $\Omega_x(x_3^2)$ will make the model locally unstable ; but when $\partial\Omega_x/\partial x_3 < 0$, a feature that distinguishes some of the models (§ 6, middle region of Figure 1), we certainly have local stability.

5. THE NORMALIZATION USED

In Paper I, the equilibrium was worked out normalizing the gravitational potential, the angular velocity, and the length. This time we essentially do the same, but now adding a velocity and a time normalization. Thus, we take

$$v^1 = \frac{v}{v_0}, \quad x^1 = \frac{x}{a_1}, \quad t^1 = \frac{v_0}{a_1}\,t, \quad V^1 = \frac{V}{G\rho a_1^2}, \quad \chi^1 = \frac{\chi}{G\rho a_1^4}, \quad p^1 = \frac{p}{v_0^2\rho}, \tag{14}$$

where v is velocity, x length, t time, V potential, χ super-potential, and p pressure, a_1 being the largest semi-axis. Here, we seek at best to preserve the (quadratic) angular velocity Ω and other variables as they were used in Paper I. For this purpose, we take

$$v_0 = a_1\sqrt{G\rho}, \tag{15}$$

so that $\omega = \sqrt{G\rho}\sqrt{\Omega^1}$, the new Ω^1 being twice the old one. In what follows, normalized variable indices will be omitted.

6. A CORRECTION TO PAPER I

In Paper I, an omission of a factor r in our spheroidal figures computing program for Ω was tardily found, resulting in an erroneous Ω for the spheroidal figures, although it is qualitatively similar to the correct one. Applying the procedure explained here we reconstructed Ω for the series corresponding to $d = 1/8$ and $d = -1/8$ (Tables 1 and 2). For $d = 1/8$, the angular velocity distribution qualitatively remains as in Paper I; for $d = -1/8$, although the forbidden region ($\Omega < 0$) is recuperated, we now find that the allowed region splits up into two (Figure 1; to be compared with Figure 6 of Paper I): one with increasing Ω from the equator to the pole, and the other with the inverted tendency, the transition between them not being an abrupt one. On the left of Figure 1 is shown the frontier curve separating the region where $\partial\Omega/\partial z > 0$ from the region where $\partial\Omega/\partial z < 0$. In Table 3 we give data related to the forbidden and allowed region boundaries (Figure 1).

TABLE 1

PARAMETERS $\alpha_0, \ldots, \alpha_4$ FOR DETERMINING THE ANGULAR VELOCITY DISTRIBUTION Ω^*

			$\Omega = \frac{1}{r}\alpha_s(x_3^2) + \alpha_x(x_3^2) + \alpha_y(x_3^2)r^{\mathrm{a}}$			
e_3	V_p	α_0	α_1	α_2	α_3	α_4
0.90	3.989574	-1.258680	0.698978	5.278133	- 7.782012	- 4.111402
0.80	3.777258	-0.839818	0.560006	3.288077	- 5.550472	- 2.498456
0.70	3.533861	-0.589118	0.485767	2.142312	- 3.970951	- 1.581472
0.60	3.252625	-0.478838	0.500581	1.610184	- 2.911622	- 1.149477
0.40	2.538777	0.408187	- 0.648867	- 1.139885	1.022249	0.738790
0.30	2.079107	0.100747	- 0.156568	- 0.259099	0.422920	0.159540
0.20	1.524583	0.047562	- 0.051667	- 0.113459	0.432160	0.066219
0.10	0.845626	0.015314	- 0.005222	-0.032916	0.321363	0.017581
0.05	0.446944	-0.003803	0.003386	0.012272	0.189735	- 0.008641

*For the series e_3, $d = 1/8$. The potential V_p at the pole is included.

[a]α_s, α_x, α_y are related to $\alpha_0, \ldots, \alpha_4$ through equation (7) and the condition $\alpha_s(z_M) = 0$.

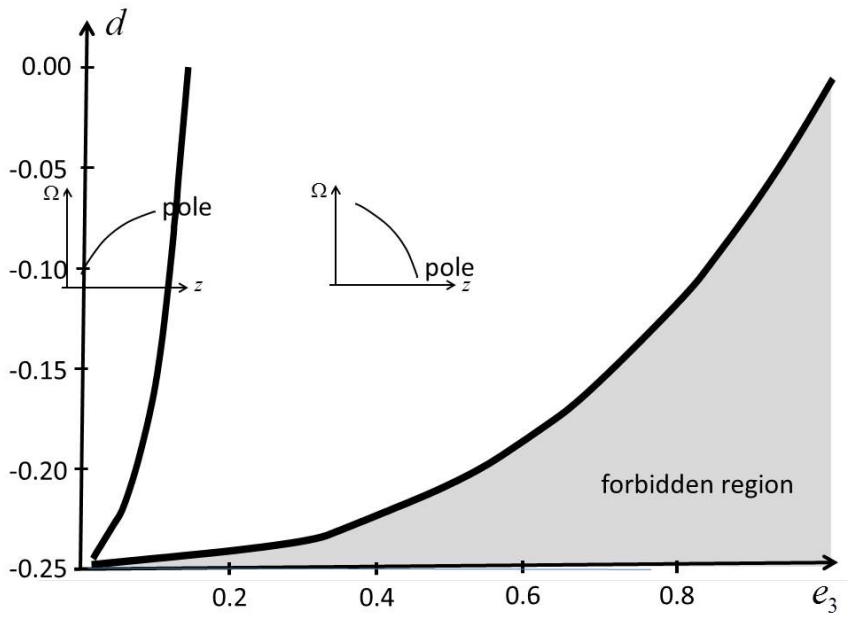

Fig. 1. d-curves in the range of negative values separating spheroidal figures with $\Omega > 0$ from those with $\Omega < 0$ (shaded area), and figures with increasing Ω from those with decreasing Ω, from equator to pole.

7. VIRIAL TECHNIQUE TO SECOND-HARMONIC

The nine second order virial equations for fluid motion are (Tassoul & Ostriker, 1968):

$$\frac{d}{dt}\int_\tau v_i x_j \, d\tau = 2T_{ij} + W_{ij} + \Pi\delta_{ij}, \tag{16}$$

TABLE 2

PARAMETERS $\alpha_0, \ldots, \alpha_4$ FOR DETERMINING THE ANGULAR VELOCITY DISTRIBUTION Ω^*

			$\Omega = \frac{1}{r}\alpha_s(\,x_3^2) + \alpha_x(\,x_3^2) + \alpha_y(\,x_3^2)r^{\rm a}$			
e_3	V_p	α_0	α_1	α_2	α_3	α_4
0.95	forbidden					
0.90	forbidden					
0.80	forbidden					
0.70	3.593729	- 0.133209	- 0.041356	0.652807	- 2.693034	- 0.539688
0.60	3.331374	- 0.017090	- 0.002801	0.074007	- 1.658608	- 0.058820
0.50	3.019679	0.009859	0.088398	- 0.070746	- 1.030713	0.064056
0.40	2.645115	- 0.192470	0.563862	0.785828	- 1.519715	- 0.618194
0.30	2.189056	0.197253	- 0.169552	- 0.701692	0.551031	0.517770
0.20	1.625176	0.126071	- 0.070154	- 0.440562	0.531001	0.323031
0.10	0.915033	0.054159	- 0.021556	- 0.191738	0.381757	0.141496
0.05	0.487934	0.005433	- 0.006491	- 0.030662	0.222023	0.026296

*For the series e_3, $d = -1/8$. The potential V_p at the pole is included.

[a]α_s, α_x, α_y are related to $\alpha_0, \ldots, \alpha_4$ through equation (7) and the condition $\alpha_s(z_M) = 0$.

TABLE 3

e_{3a}, e_{3f}, AND PARAMETER d^*

e_{3a}	e_{3f}	d
0.159	0.925	-0.050
0.147	0.835	-0.100
0.132	0.718	-0.150
0.105	0.549	-0.200
0.075	0.376	-0.230
0.050	0.206	-0.245

*For the limit curves in allowed (a) and forbidden (f) region, Figure 1.

where all variables are normalized ($G\rho = 1$, and so on) and

$$T_{ij} = \frac{1}{2}\int_\tau v_i v_j \, d\tau, \quad W_{ij} = -\frac{1}{2}\int_\tau B_{ij}\, d\tau = -\frac{1}{2}\int_\tau\int_\tau \frac{(x_i - x_i')(x_j - x_j')}{|\mathbf{x} - \mathbf{x}'|^3}\, d\tau d\tau', \tag{17}$$
$$\Pi = \int_\tau p \, d\tau.$$

To carry out our stability analysis, an equilibrium state must be taken as a starting point and then small departures from it considered. The perturbed flow is characterized by a small Lagrangian displacement $\boldsymbol{\xi}(\mathbf{x}, t)$, in terms of which the virial equations to the first order in $\boldsymbol{\xi}$ become (Chandrasekhar, 1965)

$$\frac{d}{dt}\int_V (\triangle v_i x_j + v_i \xi_j)\, d\tau = 2\,\delta T_{ij} + \delta W_{ij}, \tag{18}$$

where δ is the variation of the integrals corresponding to the variables, and

$$\triangle v_i = \frac{\partial \xi_i}{\partial t} + v_j \frac{\partial \xi_i}{\partial x_j}. \tag{19}$$

Sum over repeated indices is understood and variables (like v_j) accompanying terms in ξ are equilibrium variables (independent of time, in our case). The interest here is on the proper oscillations of the figure and for this reason we propose $\boldsymbol{\xi}$ as

$$\boldsymbol{\xi}(\mathbf{x},t)=\boldsymbol{\xi}(\mathbf{x})e^{\lambda t}. \tag{20}$$

If the eigenvalue λ is positive the equilibrium state will be unstable; if it is negative the motion will be damped; if λ is imaginary we have a stable oscillatory motion. To simplify the analysis we make the approximation (Chandrasekhar & Lebovitz, 1962, 248; Tassoul & Ostriker, 1968)

$$\xi_i(\mathbf{x})=L_{ij}x_j, \tag{21}$$

where L_{ij} is a set of nine constants to be determined. The nine second order virial equations are thus

$$\lambda^2 L_{i\underline{j}}\int x_{\underline{j}}^2\,d\tau-2\lambda L_{ik}\int\sqrt{\Omega}\epsilon_{jk}x_k^2\,d\tau+L_{ik}\int\Omega\epsilon_{jl}\epsilon_{lk}x_k^2\,d\tau+L_{jk}\int\Omega\epsilon_{il}\epsilon_{lk}x_k^2\,d\tau=-L_{kl}W_{lk;ij}. \tag{22}$$

$\epsilon_{12}=-1$, $\epsilon_{21}=1$ and $\epsilon_{ij}=0$ for the remaining cases. The super-matrix $W_{lk;ij}$ is defined as (Chandrasekhar & Lebovitz, 1962, 238)

$$W_{lk;ij}=\int x_l\frac{\partial B_{ij}}{\partial x_k}\,d\tau, \tag{23}$$

and

$$B_{ij}=\int\frac{(x_i-x_i')(x_j-x_j')}{|\mathbf{x}-\mathbf{x}'|}\,d\tau'=V\,\delta_{ij}+\frac{\partial^2\chi}{\partial x_i\partial x_j}. \tag{24}$$

According to our figure's symmetry only 7 of the 81 super-matrix components are unequal and different from zero, namely:

$$W_{11;11},\quad W_{33;33},\quad W_{11;22},\quad W_{11;33},\quad W_{12;12},\quad W_{13;13},\quad W_{31;13}. \tag{25}$$

The remaining non-vanishing components are related to these by

$$\begin{aligned}
&W_{22;22}=W_{11;11},\quad W_{22;11}=W_{11;22},\quad W_{33;11}=W_{11;33},\quad W_{22;33}=W_{11;33},\\
&W_{33;22}=W_{11;33},\quad W_{12;21}=W_{12;12},\quad W_{21;21}=W_{12;12},\quad W_{21;12}=W_{12;12},\\
&W_{13;31}=W_{13;13},\quad W_{31;31}=W_{13;13},\quad W_{31;13}=W_{13;13},\quad W_{23;32}=W_{31;13},\\
&W_{32;32}=W_{31;13},\quad W_{32;23}=W_{31;13}.
\end{aligned} \tag{26}$$

According to equations (5), (7) and (8), the potential V and the super-potential χ are known and we are now ready for calculating the necessary $W_{pq;ij}$ components.

For easy writing, we abbreviate

$$J_1=\int x_1^2\,d\tau,\quad J_2=\int x_2^2\,d\tau=J_1,\quad J_3=\int x_3^2\,d\tau,\quad \Omega_1=\int\sqrt{\Omega}x_1^2\,d\tau,\quad \Omega_2=\int\Omega x_1^2\,d\tau, \tag{27}$$

so that equations (22) become

$$\lambda^2 L_{i\underline{j}}I_{\underline{j}}-2\lambda\Omega_1 L_{ik}\epsilon_{jk}+\Omega_2 L_{ik}\epsilon_{jl}\epsilon_{lk}+\Omega_2 L_{jk}\epsilon_{il}\epsilon_{lk}=-L_{kl}W_{lk;ij}. \tag{28}$$

This is an homogeneous equation system in L_{ij} whose determinant must be zero in order to have a non-trivial solution. Instead of working with the whole determinant we solve subsystems, as is commonly done. This is possible by first noticing that the unknowns L_{13}, L_{23}, L_{31} and L_{32}, and only these, are present in four of the equations, which bring us to the first oscillation type.

7.1. *Transverse-shear modes*

These modes are related to the displacements according to

$$\xi_1=L_{13}x_3,\quad \xi_2=L_{23}x_3,\quad \xi_3=L_{31}x_1+L_{32}x_2,$$

and the corresponding equation system is

$$\begin{aligned} L_{31}\left(W_{13;13}-\Omega_2\right)+L_{13}\left(W_{31;13}+J_3\lambda^2\right)&=0,\\ L_{32}\left(W_{13;13}-\Omega_2\right)+L_{23}\left(W_{31;13}+J_3\lambda^2\right)&=0,\\ L_{31}\left(W_{13;13}+J_1\lambda^2-\Omega_2\right)+L_{13}W_{31;13}+2L_{32}\lambda\Omega_1&=0,\\ L_{32}\left(W_{13;13}+J_1\lambda^2-\Omega_2\right)+L_{23}W_{31;13}-2L_{31}\lambda\Omega_1&=0\,, \end{aligned} \tag{29}$$

whose determinant must be zero:

$$\sigma^2\left(B-M-L+\sigma^2\right)^2-4A^2\left(M-\sigma^2\right)^2=0, \tag{30}$$

where

$$\lambda=i\,\sigma,\quad A=\frac{\Omega_1}{J_1},\quad B=\frac{\Omega_2}{J_1},\quad M=\frac{W_{31;13}}{J_3},\quad L=\frac{W_{13;13}}{J_1}. \tag{31}$$

Equation (30) is the eigenfrequency dispersion relation.

7.2. *Toroidal modes*

The remaining five equations are

$$L_{11}\left(W_{11;11}-2J_1B+J_1\lambda^2\right)+L_{22}W_{11;22}+L_{33}W_{11;33}+2J_1AL_{12}\lambda=0, \tag{32}$$

$$L_{22}\left(W_{11;11}-2J_1B+J_1\lambda^2\right)+L_{11}W_{11;22}+L_{33}W_{11;33}-2J_1AL_{21}\lambda=0, \tag{33}$$

$$L_{33}\left(W_{33;33}+J_3\lambda^2\right)+L_{11}W_{11;33}+L_{22}W_{11;33}=0, \tag{34}$$

$$L_{12}\left(W_{12;12}-J_1B+J_1\lambda^2\right)+L_{21}\left(W_{12;12}-J_1B\right)-2J_1AL_{11}\lambda=0, \tag{35}$$

$$L_{21}\left(W_{12;12}-J_1B+J_1\lambda^2\right)+L_{12}\left(W_{12;12}-J_1B\right)+2J_1AL_{22}\lambda=0. \tag{36}$$

and these can be handled for obtaining the toroidal modes. Subtracting equation (32) from (33) and adding equations (35) and (36) we obtain a system in the two variables $(L_{11}-L_{22})$ and $(L_{12}+L_{21})$, whose solution is subjected to the vanishing of the determinant ($\lambda=i\,\sigma$ and $2\,W_{12;12}=W_{11;11}-W_{11;22}$):

$$\sigma^4-4\left(\frac{W_{12;12}}{J_1}+A^2-B\right)\sigma^2+4\left(\frac{W_{12;12}}{J_1}-B\right)^2=0. \tag{37}$$

Stable oscillatory motion is possible whenever $\sigma^2\geq 0$; neutral modes ($\sigma=0$) result if

$$B=\frac{W_{12;12}}{J_1},\quad \text{or}\quad \Omega_2=W_{12;12}. \tag{38}$$

7.3. *Pulsatory mode*

We come to the last mode following a typical procedure for incompressible fluids (Chandrasekhar, 1969, p. 84). Adding equations (32) and (33), and subtracting twice equation (34), one obtains

$$\begin{aligned} &\left(L_{11}+L_{22}\right)\left(W_{11;11}+W_{11;22}-2W_{11;33}-2BJ_1+J_1\lambda^2\right)-2L_{33}\left(-W_{11;33}\right.\\ &\left.+W_{33;33}+J_3\lambda^2\right)+2AJ_1\lambda\left(L_{12}-L_{21}\right)=0. \end{aligned} \tag{39}$$

Subtracting now equation (35) from (36), there results

$$J_1\lambda\left(L_{12}-L_{21}\right)-2AJ_1\left(L_{11}+L_{22}\right)=0. \tag{40}$$

Finally we eliminate $L_{12}-L_{21}$ and $L_{11}+L_{22}$ from equation (39) with the help of equation (40) and Chandrasekhar's Theorem 17 (Chandrasekhar, 1969, p. 61) based on the figure's form and the continuity equation ($\operatorname{div}\boldsymbol{\xi}=0$), that for our particular figure is

$$L_{11}+L_{22}=-\left(4d\frac{J_{33}}{J_1e_3^4}+\frac{J_3}{J_1e_3^2}\right)L_{33}, \tag{41}$$

where

$$J_{33} = \int x_3^4 \, d\tau. \tag{42}$$

From the last result one arrives at the dispersion relation

$$\sigma^2 = \frac{C\left(W_{11;11} + W_{11;22} - 2W_{11;33} + 4A^2 J_1 - 2BJ_1\right) + 2W_{11;33} - 2W_{33;33}}{CJ_1 - 2J_3}, \tag{43}$$

meaning

$$C = -\left(4d\frac{J_{33}}{e_3^4 J_1} + \frac{J_3}{e_3^2 J_1}\right).$$

8. NUMERICAL RESULTS

8.1. *Stability of figures with cylindrical angular velocity distribution*

The various oscillatory modes can be calculated from the figure's equilibrium state, namely, for given d, e_3 and V_p (pole angular velocity); once these quantities have been determined the surface angular velocity distribution (equation (9)) can be extended from the surface inward. Next, the potential and super-potential expressions can be numerically evaluated, as explained in § 3, and the Ω integrals (in equation (27)) along with the $W_{pq;ij}$ elements (equations (23), (24) and (25)) can be established.

As an illustration we have worked out two particular cases: $d = 1/8$ and $d = -1/8$ (see Tables 1 and 2). With equations (30), (37) and (43), one builds Tables 4 and 5 for the transverse-shear modes (σ_1, σ_2 and σ_3), the toroidal modes (σ_4 and σ_5) and the pulsatory mode (σ_6). The entries for σ_4 corresponding to the neutral point, and the beginning of the instability regime, are given with five significative figures.

TABLE 4

PROPER FREQUENCIES $\sigma_1, \sigma_2, \sigma_3$ (TRANSVERSE-SHEAR MODES), σ_4, σ_5 (TOROIDAL MODES) AND σ_6 (PULSATORY MODE)[a]

e_3	σ_1	σ_2	σ_3	σ_4	σ_5	σ_6
0.9	0.7579	1.5240	2.2879	0.8115	2.3333	2.0034
0.8	0.9135	1.4788	2.4005	0.4923	2.3275	2.0948
0.7	1.0303	1.4438	2.4856	0.1925	2.2644	2.1651
0.63432	1.0989	1.4179	2.5311	0.0000	2.1918	2.2013
0.6	1.1160	1.4102	2.5407	0.1001	2.1464	2.2039
0.5	1.1701	1.3703	2.5592	0.3960	1.9631	2.1942
0.4	1.1884	1.3162	2.5283	0.7216	1.6789	2.1115
0.32861	1.1749	1.2623	2.4626	$1.1876 \pm 0.0\, i$		1.9924
0.3	1.1607	1.2344	2.4226	$1.1744 \pm 0.2795\, i$		1.9278
0.2	1.0606	1.0991	2.1968	$1.0792 \pm 0.5179\, i$		1.6017

[a]For the spheroidal figure characterized by e_3, $d = 1/8$ and a cylindrical angular velocity distribution. The model with $e_3 = 0.63432$ has a zero frequency (branch model), and $e_3 = 0.32861$ is the instability onset. The physical frequencies are the given ones multiplied by $\sqrt{G\,\rho}$ (equation (14)).

For the toroidal oscillation modes one has $\xi_1 = L_{11}x_1 + L_{12}x_2$, $\xi_2 = L_{21}x_1 + L_{22}x_2$ and $\xi_3 = 0$, so that a figure's circular section $x_1^2 + x_2^2 = r$ is distorted to

$$(1 + 2L_{11})\, x_1^2 + 2(L_{12} + L_{21})\, x_1^2 x_2^2 + (1 + 2L_{22})\, x_2^2 = r,$$

neglecting smaller square L-terms as compared to L. This is the ellipse equation, so that a circle is converted back and forth into an ellipse by the perturbation. For a neutral mode ($\sigma_4 = 0$), the perturbed circle permanently

TABLE 5

PROPER FREQUENCIES $\sigma_1, \sigma_2, \sigma_3$ (TRANSVERSE-SHEAR MODES), σ_4, σ_5 (TOROIDAL MODES) AND σ_6 (PULSATORY MODE)*

e_3	σ_1	σ_2	σ_3	σ_4	σ_5	σ_6
0.7	0.7692	1.5338	2.2878	0.7303	2.2535	2.0651
0.6	0.9559	1.4707	2.4064	0.3332	2.2247	2.1531
0.50929	1.0774	1.4184	2.4645	0.0000	2.1235	2.2071
0.5	1.0860	1.4128	2.4693	0.0342	2.1083	2.2083
0.4	1.1643	1.3535	2.4819	0.4009	1.8917	2.1852
0.3	1.1887	1.2749	2.4153	0.8224	1.5066	2.0569
0.26620	1.1827	1.2408	2.3674	1.1546 ±0 .0 i		1.9819
0.2	1.1387	1.1562	2.2244	1.1034 ±0 .4369 i		1.2947
0.1	0.9537	0.9724	1.7836	0.0912 ±0 .5294 i		1.2464

*For the spheroidal figure characterized by e_3, $d = -1/8$ and cylindrical angular velocity distribution.[a]

[a]Model with $e_3 = 0.50929$ has a zero frequency (branching model), and $e_3 = 0.26620$ is the instability onset. The physical frequencies are the given ones multiplied by $\sqrt{G\,\rho}$ (equation (14)).

TABLE 6

PROPER FREQUENCIES $\sigma_1, \sigma_2, \sigma_3$ (TRANSVERSE-SHEAR MODES), σ_4, σ_5 (TOROIDAL MODES) AND σ_6 (PULSATORY MODE)*

e_3	σ_1	σ_2	σ_3	σ_4	σ_5	σ_6
0.90			forbidden			
0.80			forbidden			
0.70	0.8333	1.5089	2.3270	0.6334	2.2847	2.0888
0.60	0.9970	1.4556	2.4321	0.2617	2.2351	2.1735
0.525618	1.0879	1.4174	2.4772	0.0000	2.1477	2.2164
0.50	1.1129	1.4033	2.4863	0.0889	2.1071	2.2251
0.40	1.1810	1.3478	2.4925	0.4432	1.8824	2.1980
0.30	1.1973	1.2720	2.4207	0.8612	1.4849	2.0650
0.272133	1.1902	1.2449	2.3819	1.1636 ± 0.0 i		2.0015
0.2	1.1410	1.1554	2.2258	1.1067 ± 0.4425 i		1.7695

*For the spheroidal figure characterized by e_3, $d = -1/8$ and a disklike angular velocity distribution.[a]

[a]Model with $e_3 = 0.525618$ has $\sigma_4 = 0$; onset of instability is at $e_3 = 0.272133$. The frequencies are normalized to $\sqrt{G\,\rho}$ (equation (14)).

remains as an ellipse. In our case the neutral frequency marks, in actual fact, a bifurcation point where a series of ellipsoidal figures branches off; this can be verified by observing Table 1 of Paper I for ellipsoidal figures ($d = 1/8$) whose first row corresponds to a nearly spheroidal form ($e_2 = 0.99 \approx 1$), for which $e_3 = 0.6574$; this value is similar to the value of the neutral frequency, namely, $e_3 = 0.6343$. For $d = -1/8$ (not reported in Paper I), we now know that the spheroidal limit is located at $e_3 = 0.4657$, near to $e_3 = 0.5093$ (Table 5) where the neutral frequency occurs. These values do not exactly agree due to the imprecision of the virial technique as applied to our distorted models.

According to Tables 4 and 5, for low d the neutral point is located at a lower z_M value. More generally, numerical results show that for neutral points z_M increases with increasing d, so that the figures become less flattened, a conclusion reached by obtaining the neutral points when $d = -1/5, -1/8, -1/16,\ 1/16, 1/8, 1/5$.

Interpolating our results to $d = 0$, we obtain $e_3 = 0.5831$ which is very close to Chandrasekhar's $e_3 = 0.5827$ for Maclaurin spheroids (Chandrasekhar, 1969, p. 85).

8.2. *Stability of figures with disklike angular velocity distribution*

To discuss this case we take the series for $d = -1/8$, which spans from about $e_3 = 0.3$ to $e_3 = 0.7$ (for $e_3 \gtrsim 0.7$ the figures are forbidden) with the property $\partial\Omega/\partial x_3 = \partial\Omega(x_3^2)/\partial x_3 < 0$; for $e_3 < 0.3$ we have models with $\partial(s^2\omega)/\partial x_3 > 0$ (see equation (12) and Figure 1) and the disklike distribution is unsuitable. Results for transverse-shear modes (σ_1, σ_2 and σ_3), toroidal modes (σ_4 and σ_5) and pulsatory mode (σ_6) are given in Table 6; the frequencies are plotted in Figure 2. Figure 2 shows that the onset of instability is located at $e_3 \approx 0.27$, ($\sigma_4 = \sigma_5$), and the neutral frequency is located at $e_3 \approx 0.53$. Here again the figure with neutral frequency represents the bifurcation of an ellipsoidal sequence. The $d = -1/8$ ellipsoidal series has a limiting figure at $e_3 = 0.4657$ (see previous Section), whereas the corresponding neutral frequency occurs at $e_3 = 0.5256$, and the difference between the two values is even greater than that for the cylindrical distribution. Therefore, the precision of assumption (21) depends on the angular velocity distribution.

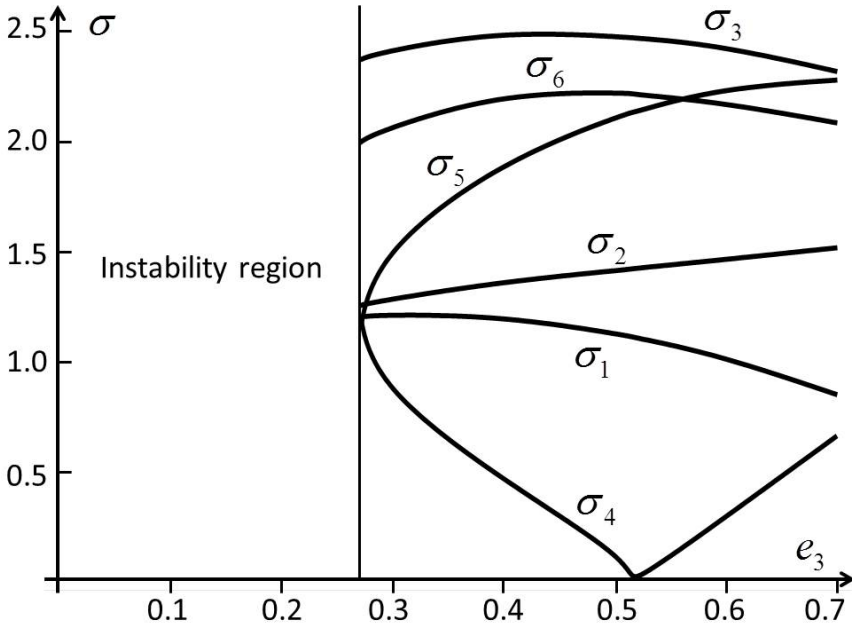

Fig. 2. Frequencies for the series $d = -1/8$ and disklike angular velocity distribution, ranging from $e_3 = 0.27$ (end of instability interval) to $e_3 = 0.7$ (start of forbidden region, Figure 1).

REFERENCES

Chandrasekhar, S. & Lebovitz, N. R. 1962, ApJ, 135, 238

Chandrasekhar, S. & Lebovitz, N. R. 1962, ApJ, 135, 248

Chandrasekhar, S. 1965, ApJ, 141, 1043

Chandrasekhar, S. 1969, Ellipsoidal Figures Of Equilibrium (New Haven: Yale University Press)

Cisneros, J. U., Martínez, F. J., & Montalvo, J. D. 2015, RMxAA, 51, 119 (Paper I)

Dryden, H. L., Murnaghan, F. P., & Bateman, H. 1956, Hydrodynamics (Ney York: Dover Publications Inc.)

Goldreich, P. & Schubert, G. 1967, ApJ, 150, 571

Tassoul, J. L. & Ostriker, J. P. 1968, ApJ, 154, 613

Francisco J. Martínez Herrera and J. Daniel Montalvo Castro: Instituto de Física, Universidad Autónoma de San Luis Potosí, Zona Universitaria s/n, 78290 San Luis Potosí, S.L.P., México.

Joel U. Cisneros Parra: Facultad de Ciencias, Universidad Autónoma de San Luis Potosí, Zona Universitaria s/n, 78290 San Luis Potosí, S.L.P., México (cisneros@galia.fc.uaslp.mx).